# Fabrication of optical microstructures on roller surface based on fast tool servo system

*Chaoliang Guan, Jiahao Yong, Junfeng Liu ✉, Yifan Dai, Zhanbin Fan, Fei Li*

*Laboratory of Science and Technology on Integrated Logistics Support, National University of Defense Technology, Changsha 410073, People's Republic of China*
✉ *E-mail: ljf20090702122@163.com*

Published in Micro & Nano Letters; Received on 17th April 2020; Revised on 18th June 2020; Accepted on 30th June 2020

The optical microstructure on the roller surface is the key for manufacturing microstructures on optical film. In this context, the fabrication of optical microstructures on the cylindrical roller surface is more difficult than that on the planar surface. This Letter starts with a machinability of microstructure arrays on a cylindrical surface, and studies the restriction influences of the tool geometry and process parameters on the characteristics of the microstructure. Then a suitable flexible hinge holder for the fast tool servo is designed based on finite element analysis, and the influential factors to the machining precision of microstructure arrays are investigated. Finally, a machining test of spherical arrays on an aluminium cylindrical surface is carried out, and the high quality of the microstructure indicates that the proposed method is appropriate for the fabrication of optical microstructures.

**1. Introduction:** The optical films with various forms of microstructures are widely used in liquid crystal display, LED lighting, optical instruments and other fields of application, and play an important role in the development of science technology and global economy [1, 2]. The roller is the key part of the moulding of microstructure optical films, and its surface is inscribed with a lot of microstructures, such as micro-sphere arrays, Fresnel structure array, prism array, pyramids array etc. The optical microstructures are hard to fabricate due to the complicated structure and high requirements of shape precision and surface roughness [3], and the mainstream process technology is the ultra-precision turning combined with fast tool servo (FTS) [4]. In general, the manufacturability with turning, the consistency across numerous microstructures and the restriction of the dynamic behaviour of FTS catch the most attention [5].

America and Germany are leading the way in the field of ultra-precision machining for surface microstructures. For example, the various roll lathes of PRECITECH and KUGLER are highly commercialised. The advanced manufacturing research department of Korean machinery and materials society performed the design, simulation and evaluation for the roller lathe, and processed the microstructures of cutting prism with high quality [6]. The National University of Defense Technology had done massive works in the fabrication of microstructures on the end face with their self-developed FTS system, such as sinusoidal radiation, sinusoidal phase plane and micro-lens array, in which the surface roughness of the lens array with circumferential arrangement reaches to 11.4 nm [7].

FTS can control the tool to make a high frequency and precision reciprocating motion, which is used in the processing of microstructures in combination with a turning lathe [8]. FTS is generally supported by the piezo actuator with the advantage of high peak acceleration and bandwidth [9]. Lu *et al.* [10] developed an FTS for precision machining and discussed the influence of the clearance angle of the diamond tool on the microstructure shape accuracy. With the modification of the tool path, Yu *et al.* [11] proposed a compensation method to pre-compensate the induced profile errors in FTS diamond turning, and effectively improved the machining precision of microstructures. To predict the microstructure generation, Lu *et al.* [12] presented a way for calculating the microstructure profile amplitude and wavelength, and conducted the cutting test to verify the proposed method. Zhu *et al.* [13] investigated the feasibility of a novel quasi-elliptical tool servo for the vibration suppression in the turning of micro-lens arrays, and significantly eliminate the tool vibration caused by the non-smooth servo motion of the FTS. Based on an error-correcting algorithm, Wang and Li [14] carried out a lens arrays with 0.06 μm in peak-to-valley value of form error using FTS system. To effectively reduce the overcut of the lens edge, Liu *et al.* [15] proposed an optimisation method of tool path generation with the interpolation of the lens edge.

Those research studies above extensively discussed the machining equipment, processing technics, error compensation methods and precision evaluation for microstructures on planar surfaces, while in the processing of optical films with microstructures on roller surface, the generation of microstructure arrays on a cylindrical surface. Moreover, the join between the adjacent arrays along the circumferential direction becomes a technical difficulty. In response, this Letter studies the machining feasibility of the microstructures on the cylindrical surface and discusses the influence factors in the process, and the proposed machining technic is experimentally validated based on the designed FTS.

**2. Machinability of the microstructures on cylindrical surface:** The fabrication of the microstructures on the cylindrical surface is restricted by the tool geometry, characteristic of FTS and process parameters, which influences the precision and quality of the finished surface. The study on the restriction rule of the machinability of those objects enables to conduct the selections of tools and process parameters.

2.1. Restriction of tool geometry: Microstructures on the cylindrical surface can be classified into two kinds according to the surface characteristic: one only relates to the reference point position along the $Z$ direction in machine coordinate system, such as microstructures of pyramids and Fresnel; another still more relates to rotation angle position $\theta$ of the reference point relative to the axis of the rotational spindle, such as microstructures of sinusoidal grids, sphere and aspherics. The surface equation of the second kind of microstructures can be written as $s = f(z, \theta)$.

In the processing, the cylindrical surface can be regarded as a plane derived from the extended cylindrical surface. The analysis of the tool restriction is based on this surface and the tool nose angle $\varepsilon$, the tool nose radius $r_\varepsilon$, rake angle $\gamma$ and tool clearance $\alpha$. Fig. 1 shows the cutting conditions of the tool along axial direction at a given time. $f_z'$ is the first-order partial derivative of the surface equation $s$ with respect to $z$; $v_c$ is the cutting speed; $\varphi$ is the apex angle of the microstructure. To avoid the overcut results from the




doi: 10.1049/mnl.2020.0240

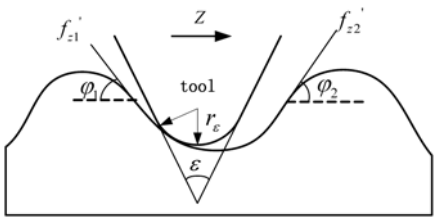


**Fig. 1** *Cutting conditions of the tool along axial directions respectively at a given time*

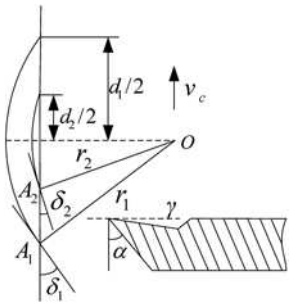


**Fig. 2** *Relationship between the tool along the cir cumferential direction and the workpiece profile*

interference between the tool and workpiece, the tool nose radius $r_\varepsilon$ must be smaller than the minimal curvature radius $\rho_{\min}$ of the section of $s$. For spherical microstructures, $\rho_{\min}=(r^2-d^2/4)^{1/2}$, where $r$ is the sphere radius and $d$ is the calibre of the microstructure. For cylindrical microstructures, $\rho_{\min}$ is equal to the cylindrical radius, while for the microstructures that consist of flat surfaces, such as linear Fresnel structure array, prism array, pyramids array etc. the tool nose angle $\varepsilon$ must be smaller than the apex angle $\varphi$ of the microstructure. The equations of the minimal curvature radii of sinusoidal and aspheric microstructures are complicated and can be calculated with MATLAB software [7].

Fig. 2 presents the relationship between the tool along the circumferential direction and the workpiece profile of spherical microstructures. In the descent phase of the tool on the workpiece surface with the sphere radius $r_1$, the included angle $\delta_1$ between the arc tangent and $v_c$ at the endpoint $A_1$ is maximal, where the possibility of the interference with the tool is maximal. Likewise, the included angle on the workpiece surface at the endpoint $A_2$ with the sphere radius $r_2$ is $\delta_2$, and $\delta_1>\delta_2$. Thus, the tool clearance $\alpha$ must be larger than the maximal included angle between the arc tangent and $v_c$, whose mathematical expression can be written as:

$$\delta_{\max}=\arcsin\left(d/(2r)\right)/\pi\times 180 \tag{1}$$

The $\delta_{\max}$ in (1) of sinusoidal and aspheric microstructures can be referred to [16]. For the microstructures consisting of flat surfaces, the sum of angles of $\alpha$ and $\varphi$ is larger than $\pi/2$.

In the rising phase of the structure, the include angle between the arc tangent and $v_c$ at any point is smaller than 90°, while for cutting ductile materials $\gamma$ is larger than or equal to 0°, so there is no interference between the front edge and the microstructure surface.

2.2. Restriction of process parameters: For microstructure arrays with periodicity along the circumferential direction, there is a restriction equation of the manufacturability between the servo tool and the microstructure:

$$\pi Dn/(60\lambda)\le B \tag{2}$$

where $D$ is the workpiece diameter; $n$ is spindle rotational speed; $\lambda$ is the microstructure period along circumferential direction; $B$ is the bandwidth of the FTS.

In the actual productive process, the work hours may be over one month, so the appropriate process parameters for improving the machining efficiency are very important. The characteristic sizes of microstructures are generally <1 mm. Fig. 3 shows the corresponding minimal bandwidths with different rotational speed and workpiece diameters under various microstructure periods. The bandwidth increases with the rotational speed and workpiece diameter, so the rotational speed can be determined by the microstructure period in the condition that the bandwidth of FTS and the workpiece diameter are known.

The machining time is equal to workpiece length $l$ divided by feed speed along the $Z$-axis $f_z$. $f_z$ is generally in the range of 0 to 5 mm/min. As shown in Fig. 4, when $f_z<1$ mm/min, the work hours for large rollers are huge, while $f_z$ is larger than 1 mm/min, the time is <48 h. Thus $f_z$ for large rollers should be chosen as large as possible on the premise of guaranteeing the machining quality.

**3. Identification of FTS system:** The FTS system is generally driven by a piezoelectric actuator and its motion is transferred by flexible hinge holder, and the hinge usually adopts the straight beam structure according to the performance requirements of FTS [15]. Fig. 5 presents the structure of straight beam hinge, and the minimum thickness $t$ and the beam length $L$ are the main parameters that affect the behaviours of the hinge holder [15]. Based on the ANSYS simulation, the influences of the main parameters on the

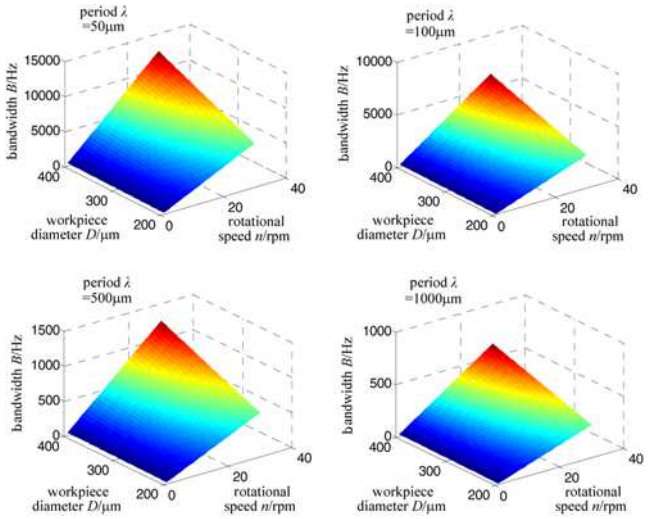


**Fig. 3** *Corresponding minimal bandwidths with different rotational speed and workpiece diameters under various microstructure periods*

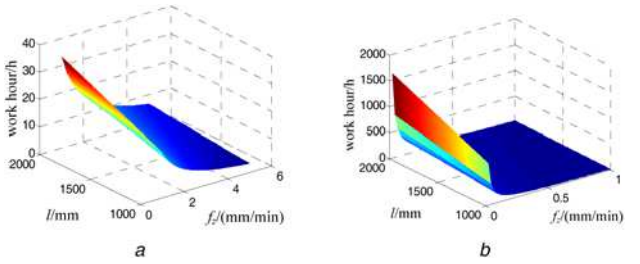


**Fig. 4** *Corresponding work hours with different workpiece lengths under various feed speeds along Z-axis*
*a* $f_z$ = 1–5 mm/min
*b* $f_z$ = 0–1 mm/min

hinge stiffness are shown in Fig. 6, and the other structural parameters are in accord with those in [15]. From the figure, it is known that the stiffness increases with minimal thickness and decreases with the beam length. According to the process requests the values of $t$ and $L$ are 0.8 and 7 mm, respectively. Fig. 7*a* shows the stress distribution with 40 μm displacement of the motion mass block of the optimised hinge, and maximum stress is far less than the yield limit; Fig. 7*b* presents the first-order mode shapes of the system, and the first natural frequency is much higher than the working frequency. The results indicate that the designed hinge is robust.

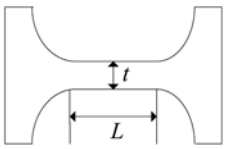


**Fig. 5** *Diagram of the hinge with the straight beam structure*

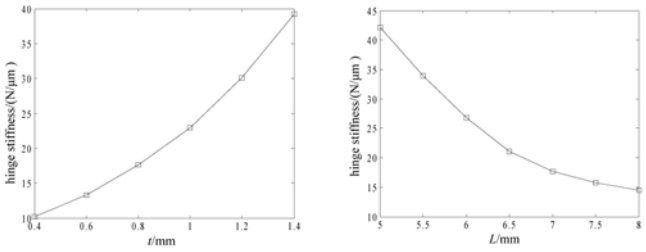


**Fig. 6** *Influences of minimal thickness and beam length on the hinge stiffness*
*a* Minimal thickness
*b* Beam length

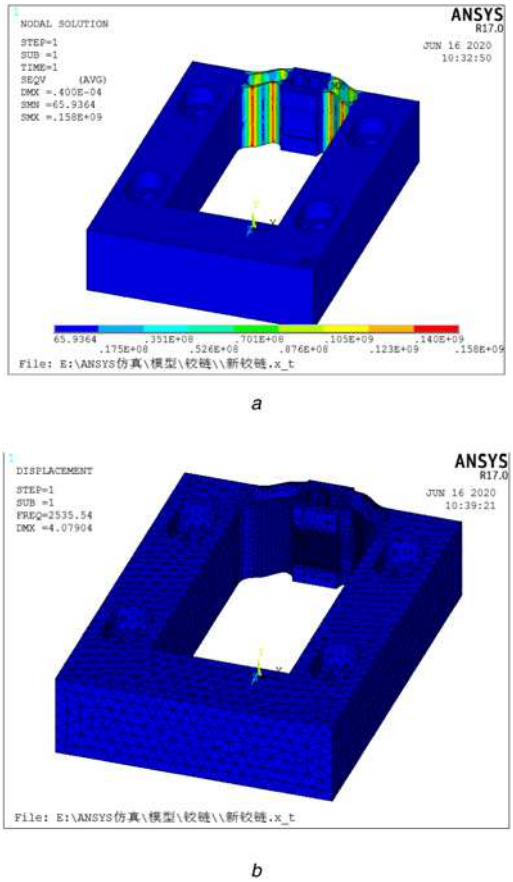


**Fig. 7** *Simulations of stress distribution and the first natural frequency*
*a* Stress distribution
*b* First mode shapes

**4. Influential factors on the machining precision:** The machining accuracy of the microstructures on the roller has a great influence on the quality of optical films, and the tool height error, overcut and temperature variation are the main factors to the machining accuracy in the manufacturing process.

4.1. Tool height error: In the manufacturing process, the initial height difference and the change of the relative position between the tool and workpiece will lead to machining error, and the machining error increases with the tool height error. In Fig. 8, $h_e$ is the tool height error; $f_t$ and $f_a$ are the theoretical and actual depths of cut, respectively; $\Delta f$ is the depth error of cut.

The following equation can be obtained by the geometric relationship:

$$\Delta f = R - \sqrt{R^2 - h_e^2} \tag{3}$$

Fig. 9 shows the relationships between the depth error of cut and the workpiece radius and tool height error. When the value of $R$ is comparatively small, the value of $\Delta f$ is relatively large and should be compensated.

4.2. Overcut: Fig. 10 presents the influence of overcut on the spherical microstructure. For discussion convenience, the geometric model of the spherical microstructure is based on the machine coordinate.

$r_m$ is the radius of a section of the sphere; $h_{max}$ is the maximum depth of the spherical microstructure; $h_m$ is the depth of a section of the spherical microstructure; $l_o$ is the value of overcut; $l_x$ is the

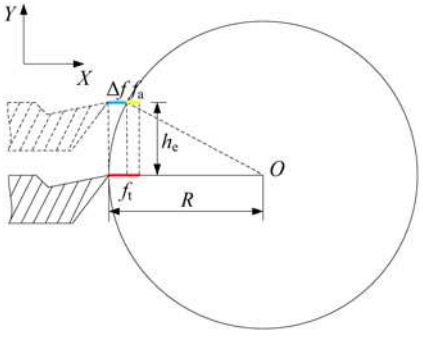


**Fig. 8** *Influence of tool height error $h_e$ on depth error of cut $\Delta f$*

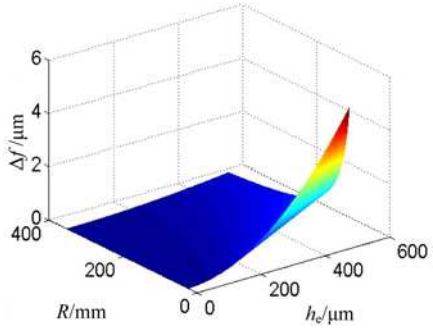


**Fig. 9** *Relationships between the depth error of cut $\Delta f$ and the workpiece radius R and tool height error $h_e$*




doi: 10.1049/mnl.2020.0240

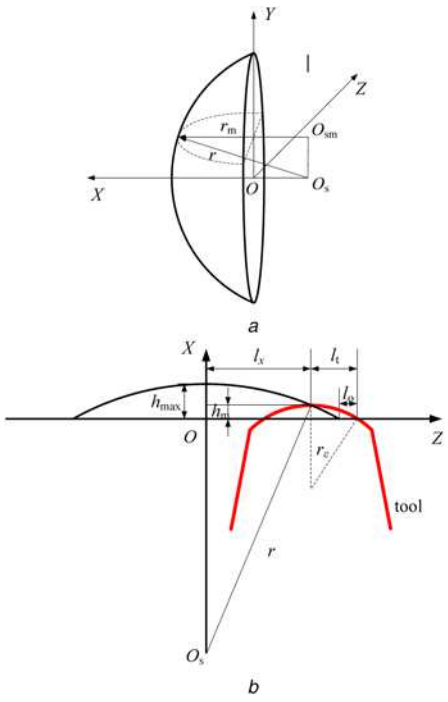


**Fig. 10** *Sketch of the overcut of spherical microstructure*
*a* Three-dimensional profile
*b* Tool position at a section in *y* direction

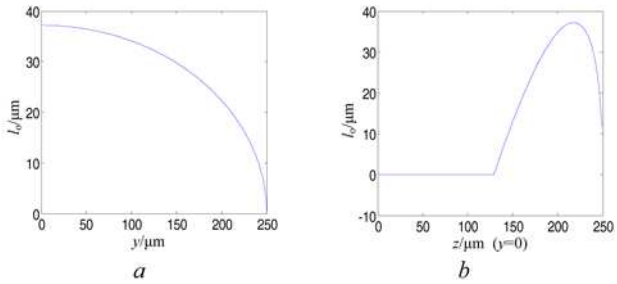


**Fig. 11** *Relationships between the overcut $l_o$ and the values in y and z directions*
*a y* direction
*b z* direction when the value in direction is zero

distance between the tool tip and *x*-axis; $l_t$ is the distance between tool tip and overcut point. Based on the geometric relationship, the overcut can be obtained by:

$$l_o = \sqrt{2r_\varepsilon\left(\sqrt{\left(\frac{d^2}{8h_{max}}+\frac{h_{max}}{2}\right)^2-y^2}-\sqrt{\left(\frac{d^2}{8h_{max}}+\frac{h_{max}}{2}\right)^2-\left(\frac{d}{2}\right)^2}\right)}-\sqrt{\left(\frac{d}{2}\right)^2-y^2}+z \tag{4}$$

Fig. 11 shows the values of $l_o$ at different coordinate points when the values of $d$, $h_{max}$ and $r_\varepsilon$ are 500 μm, 10 μm and 1 mm, respectively. It is known that the max value of $l_o$ is 37.23 μm with the coordinates of *y* and *z* axes are 0 and 318 μm, respectively.

The relationships between $l_o$ and $d$, $r_\varepsilon$ when the value of $h_{max}$ is 10 μm are shown in Fig. 12, and the value of $l_o$ increases with the

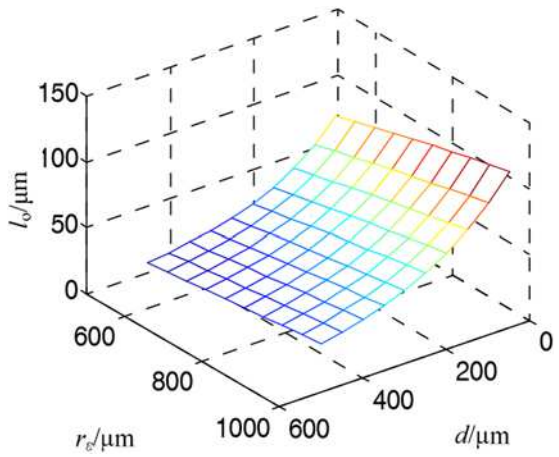


**Fig. 12** *Relationships between the overcut $l_o$ and the tool nose radius d and microstructure calibre $r_\varepsilon$*

**Table 1** Output displacement and temperature with different depths of cut

| Depth of cut, μm | 1.5 | 3.5 | 5.5 | 7.5 |
|---|---|---|---|---|
| output displacement of FTS, μm | 20.09 | 21.15 | 21.93 | 22.04 |
| temperature of hinge, °C | 20.9 | 21.1 | 21.4 | 21.5 |
| temperature of piezoelectric ceramic rod, °C | 21.2 | 22 | 22.3 | 22.4 |

values of $d$ and $r_\varepsilon$. The compensation of tool nose radius can effectively eliminate the overcut, while improves the difficulty of the control and decreases the machining efficiency.

4.3. Temperature variation: The change of output displacement of FTS results from the temperature variation affects the machining precision. The simulated machining process of spherical microstructure arrays is carried out without workpiece, and the laser displacement sensor and temperature sensor are adopted to measure the output displacement of FTS and temperature variation, respectively. Table 1 lists the output displacement and temperature with different depths of cut. The output displacement increases with the machining time and the maximum variation is 2.04 μm, and the temperature rises of the hinge and piezoelectric ceramic rod are 0.6 and 1.2°C, respectively.

**5. Processing example for microstructure on cylindrical surface:** Based on the Precitech Nanoform 350 type ultraprecision lathe and identified FTS, a processing test of spherical microstructure arrays with two distribution forms on an aluminium cylindrical workpiece with the diameter of 70 mm was carried out. The spacings of the square grids distribution along the axial and circumferential directions are both 2 mm, and that of the dislocation distribution are both 1 mm, and their simulated images are shown in Fig. 13. The calibre and depth of the spherical microstructure are 1 mm and 20 μm, respectively.

Based on the manufacturability analysis for spherical microstructures on the cylindrical surface above, the tool nose radius $r_\varepsilon$, rake angle $\gamma$ and tool clearance $\alpha$ of the selected diamond tool are 0.2 mm, 0°and 12°, respectively. The spindle rotational speed $n$ is 60 rpm and the workpiece length $l$ is 9 mm. The feed speed on the cylindrical surface and spherical surface is 0.4 and 0.2 mm/min, respectively.

The machining time for the microstructure with each distribution is about 60 min. Fig. 14 shows the machined object and microscopic photographs. There is no scratch and the spherical

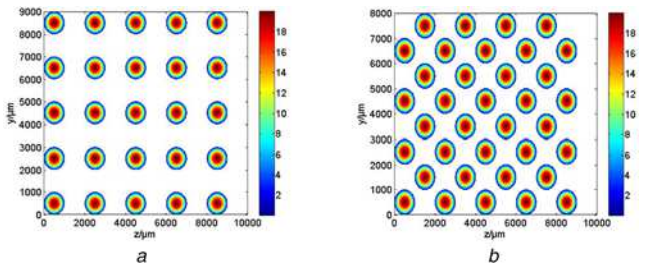

**Fig. 13** *Simulated images of spherical microstructure arrays*
*a* Square grids distribution
*b* Dislocation distribution

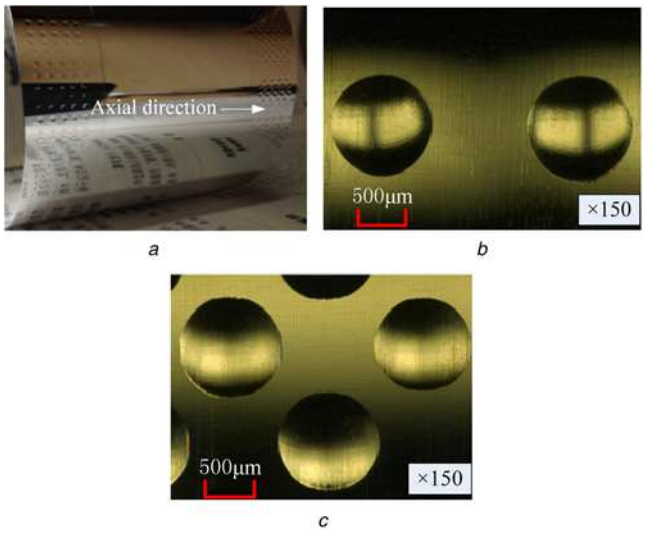


**Fig. 14** *Machined object and microscopic photographs*
*a* Machined object
*b* Square distribution
*c* Dislocation distribution

microstructures are distributed regularly on the surface, and the topography of the microstructures is clear in the microscopic photographs.

With the use of the PGI1240 type profilometer, the axial profile of the sphere surfaces in a line and the profile of the single sphere surface in the first cycle have been measured and are shown in Fig. 15. It is known that the depth of the sphere surface increases along the machining direction, and the maximum and minimum depths are 19.14 and 23.39 μm, respectively, and the general axial pitch error is 4.125 μm. The errors of depth and pitch result from the thermal displacement of FTS. The theoretical and measured curves of the single sphere surface in the first cycle are close, and the RMS and deviation of the profile are 0.0397 and 0.54 μm, respectively.

Fig. 16 presents the variations of the depth and pitch along the axial direction before and after air cooling to FTS. In the axial direction before air cooling, the depth error increases first and then appears steady, while the pitch error is large and its distribution is irregular. After air cooling, the depth error is within 0.5 μm and the pitch error decreases. Fig. 17 shows the variations of the profile deviation of the single sphere surface in the first cycle before and after air cooling to FTS, and the profile deviation is within ±0.2 μm after air cooling, which is 0.3 μm smaller than that before air cooling. From the results of Figs. 16 and 17, it is known that the air cooling to FTS can effectively improve the machining precision of the spherical microstructure arrays by controlling the temperature rise.

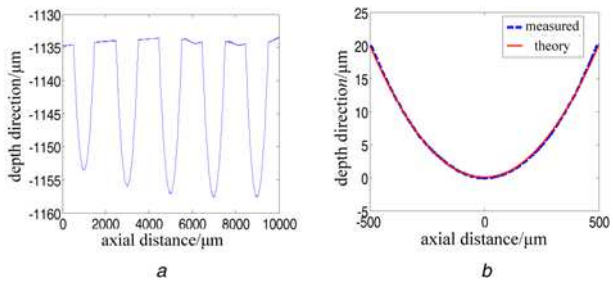


**Fig. 15** *Axial profile of the sphere surfaces in a line and profile of the single sphere surface in the first cycle*
*a* Axial profile
*b* Single profile

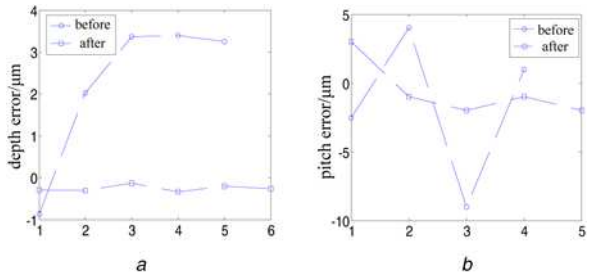


**Fig. 16** *Variations of the depth and pitch along the axial direction before and after air cooling to FTS*
*a* Depth error
*b* Pitch error

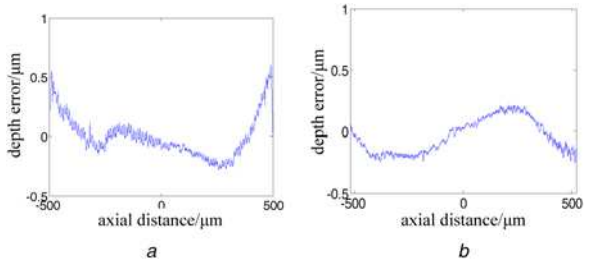


**Fig. 17** *Variations of the profile deviation of the single sphere surface in the first cycle before and after air cooling to FTS*
*a* Before air cooling
*b* After air cooling

**6. Conclusion:** The manufacturability and influence factors of optical microstructures on roller surface are investigated, and the verification test is performed on an ultra-precision lathe. From the results the following conclusions are drawn:

(a) The main structure parameters of the tool, such as the tool nose angle $\varepsilon$, the tool nose radius $r_\varepsilon$, rake angle $\gamma$ and tool clearance $\alpha$, are determined by the figure of microstructures to ensure the machining feasibility, and the feed speed along the $Z$-axis $f_z$ should be optimised to improve the machining efficiency.

(b) The minimal thickness $t$ and the beam length $L$ of the straight beam hinge are optimised by ANSYS simulation to obtain high performance of the FTS system.

(c) The tool height error $h_e$, overcut $l_o$ and temperature variation are the main factors which influence the machining precision of microstructures.




doi: 10.1049/mnl.2020.0240

(d) The fabrication of the spherical microstructure arrays on the cylindrical surface indicates the feasibility of the proposed method, and the machining precision is effectively improved by air cooling to FTS system.

**7. Acknowledgments:** This work was financially supported by the Science Challenge Project of China (No. TZ2018006-0202-03/-0102-04); the Science and Technology Foundation of State Key Laboratory (No. 6142003190101); and the Natural National Science Foundation of China (NSFC) (No. 51991372/51991371).

## 8 References

[1] Babaie J., Abolbashari M., Farahi N., *ET AL.*: 'Optical film thickness measurement of turbid materials using the fractional BiSpectrum noise-reduction technique', *Opt. Commun.*, 2009, **44**, pp. 106–116

[2] Liu C.F., Pan C.T., Chen Y.C., *ET AL.*: 'Design and fabrication of double-sided optical film for OLED lighting', *Opt. Commun.*, 2012, **22**, pp. 1–12

[3] Mochizuki H., Watanabe W., Ozeki Y.: 'Fabrication of diffractive optical elements inside polymers by femtosecond laser irradiation', *Thin Solid Films*, 2013, **291**, pp. 349–358

[4] Wang G.L., Dai Y.F., Zheng Z.W., *ET AL.*: 'Machining characteristics of complex surfaces using fast tool servo system', *Mach. Sci. Technol.*, 2011, **15**, (3), pp. 324–337

[5] Zhu W.H., Jun M.B., Altintas Y.: 'A fast tool servo design for precision turning of shafts on conventional CNC lathes', *Int. J. Mach. Tools Manuf.*, 2001, **41**, pp. 953–965

[6] Jeong S.O., Chang K.S., Jooho H., *ET AL.*: 'An ultra-precision lathe for large-area micro-structured roll molds', *J. Korean Soc. Precis. Eng.*, 2013, **30**, (12), pp. 1303–1312

[7] Fan Z.B.: 'Research on key technology in ultra-precision turning processing of microstructure on cylindrical surface' (National University of Defense Technology, CN, 2014). Published in Chinese

[8] Wu L.Q., Xu A.Q., Liao S.K.: 'Study on three degrees of freedom tandem fast tool servo device', *Mach. Tool Hydraul.*, 2017, **45**, (20), pp. 57–61. Published in Chinese

[9] Ma H.Q., Tian J., Hu D.J.: 'Development of a fast servo in noncircular turning and its control', *Mech. Syst. Signal Process.*, 2013, **41**, pp. 705–713

[10] Lu H., Choi S.C., Lee S.M., *ET AL.*: 'Microstructure of fast tool servo machining on copper alloy', *Trans. Nonferrous Met. Soc. China*, 2012, **22**, pp. s820–s824

[11] Yu D.P., Hong G.S., Wong Y.S.: 'Profile error compensation in fast tool servo diamond turning of micro-structured surfaces', *Int. J. Mach. Tools Manuf.*, 2012, **52**, pp. 13–23

[12] Lu H., Lee D., Kim J., *ET AL.*: 'Modeling and machining evaluation of microstructure fabrication by fast tool servo-based diamond machining', *Precis. Eng.*, 2014, **38**, pp. 201–216

[13] Zhu Z.W., To S., Zhu W.L., *ET AL.*: 'Feasibility study of the novel quasi-elliptical tool servo for vibration suppression in the turning of micro-lens arrays', *Int. J. Mach. Tools Manuf.*, 2017, **122**, pp. 98–105

[14] Wang G.L., Li W.X.: 'Manufacturing of lens arrays using fast tool servo system based on error correcting algorithm', *Optik*, 2019, **178**, pp. 698–703

[15] Liu C., Xue C.X., Zhang Q., *ET AL.*: 'Optimization method of tool path generation considering the edge of lenslets for a microlens array in FTS diamond turning', *Appl. Opt.*, 2019, **58**, (24), pp. 6713–6719

[16] Wen K.J., Wang G.L., Yin Z.Q.: 'Design on fast tool servo system for fine microstructures machining', *Aviat. Precis. Manu. Techn.*, 2012, **48**, (5), pp. 5–7. Published in Chinese